

Precision aggregated local models

Adam M. Edwards*

Robert B. Gramacy†

Abstract

Large scale Gaussian process (GP) regression is infeasible for larger data sets due to cubic scaling of flops and quadratic storage involved in working with covariance matrices. Remedies in recent literature focus on divide-and-conquer, e.g., partitioning into sub-problems and inducing functional (and thus computational) independence. Such approximations can be speedy, accurate, and sometimes even more flexible than an ordinary GPs. However, a big downside is loss of continuity at partition boundaries. Modern methods like local approximate GPs (LAGPs) imply effectively infinite partitioning and are thus pathologically good and bad in this regard. Model averaging, an alternative to divide-and-conquer, can maintain absolute continuity but often over-smooths, diminishing accuracy. Here we propose putting LAGP-like methods into a local experts-like framework, blending partition-based speed with model-averaging continuity, as a flagship example of what we call precision aggregated local models (PALM). Using K LAGPs, each selecting n from N total data pairs, we illustrate a scheme that is at most cubic in n , quadratic in K , and linear in N , drastically reducing computational and storage demands. Extensive empirical illustration shows how PALM is at least as accurate as LAGP, can be much faster in terms of speed, and furnishes continuous predictive surfaces. Finally, we propose sequential updating scheme which greedily refines a PALM predictor up to a computational budget.

Key words: approximate kriging neighborhoods, Gaussian process surrogate, non-parametric regression, nearest neighbor, boosting, sequential design, active learning

1 Introduction

Gaussian Processes (GPs) are popular for nonparametric modeling of non-linear functions, serving as surrogates for computer experiments (e.g., Sacks et al., 1989; Santner et al., 2018; Gramacy, 2020), models of spatially referenced data (Cressie, 1991), and as machine learners (Rasmussen and Williams, 2006). Conceptually a GP is very simple, assuming that all response values are multivariate normal (MVN) with a correlation function dictated

*Corresponding author: Department of Statistics, Virginia Tech, Hutcheson Hall, 250 Drillfield Drive Blacksburg, VA 24061, USA; adaedwar@vt.edu

†Department of Statistics, Virginia Tech

by inverse (often Euclidean) distance in the input space. While there are many ways to define the mean and covariance structure for GPs, here we use a simple default common in surrogate modeling and machine learning. Given N training data pairs (X_N, Y_N) , where X_N is comprised d -variate row vectors x_i^\top and Y_N is an N -vector of scalars, take $Y_N \sim \mathcal{N}_N(0, \tau^2(C_N + \eta\mathbb{I}_N))$, where the (i, j) coordinates of $K_N = C_N + \eta\mathbb{I}_N$ follow the so-called separable Gaussian kernel

$$K_{\theta, \eta}(x_i, x_j) = \exp \left\{ - \sum_{\ell=1}^d \frac{(x_{i\ell} - x_{j\ell})^2}{\theta_\ell} \right\} + \eta \mathbb{I}_{\{i=j\}},$$

and $\theta = (\theta_1, \dots, \theta_d)$ is the collection of *lengthscale* hyperparameters determining the strength of correlation by distance in each direction. The MVN covariance is augmented by a so-called *nugget* hyperparameter η , to allow smoothing over noisy data. Above, $\mathbb{I}_{\{i=j\}}$ is the Kroneker delta function, returning unity only when input indices match identically. We shall begin by taking a deterministic computer surrogate modeling perspective and simplify with $\eta = \epsilon$. In this context ϵ is sometimes referred to as the *jitter* (Neal, 1998).

GPs are popular because the MVN structure can be extended to new predictive locations x , where closed form conditioning yields that $Y(x) \mid (Y_N, X_N)$ is also Gaussian. Given settings of hyperparameters, moments of that distribution are given as

$$\hat{\mu}(x) = k_N^\top(x) K_N^{-1} Y_N \quad \text{and} \quad \hat{\sigma}^2(x) = \tau^2(1 + \eta - k_N^\top(x) K_N^{-1} k_N(x)), \quad (1)$$

where $k_N(x)$ is an N -dimensional column vector containing $k_\theta(x_i, x)$, for $i = 1, \dots, n$. Note that η is dropped from the subscript in k_θ because the Kroneker delta would evaluate to zero. Predictive surfaces under these equations have many desirable properties such as smoothness, and appropriate out-of-sample coverage. It can be shown that $\hat{\mu}(x)$ is a best linear unbiased predictor (BLUP), minimizing mean-squared prediction error among the class of models specified by the hyperparametrized GP kernel (see, e.g., Santner et al., 2018, Chapter 3.2). Empirically, GP predictions are hard to beat out-of-sample. Inference for θ and η proceeds via ordinary MVN log likelihoods through K_N^{-1} and $|K_N|$, perhaps leveraging closed form derivatives. Newton schemes work well (see, e.g., Gramacy, 2020, Chapter 5.2).

The big downside for GPs is evident in those equations above. Prediction and likelihood-based inference relies on decomposing a potentially large matrix $N \times N$ matrix K_N , for K_N^{-1} and $|K_N|$. Storage requirements are clearly quadratic in N , and the common Cholesky-based decomposition, yielding both inverse and determinant simultaneously, is cubic – although slight improvements are available with fancier linear algebra. Without tuned libraries such as Intel MKL, most modern workstations can cope with GPs trained on at best $N \approx 5000$. With MKL, the limit is about $N \approx 10000$ (Gramacy, 2020, Appendix A).

Work in all three GP communities – surrogate modeling, geostatistics, and machine learning – has been feverish of late, in part as an attempt to cope with the ever increasing training data sizes N produced by modern application and instrumentation. A representative, but certainly not exhaustive, list across communities includes the following: Snelson and Ghahramani (2006); Haaland and Qian (2011); Gramacy and Polson (2011); Cressie

and Johannesson (2008); Kaufman et al. (2012); Sang and Huang (2012); Nychka et al. (2002); Quiñero-Candela and Rasmussen (2005); Furrer et al. (2006); Katzfuss (2017); Katzfuss and Guinness (2018). Here our focus is on partition models, which have enjoyed considerable success in the surrogate modeling literature, for example as based on treed partitioning (Gramacy and Lee, 2008) and Voronoi tessellation (Kim et al., 2005; Rushdi et al., 2016). Although these approaches considerably expanded upon the state-of-the-art in terms of both fidelity and computation, some have taken to more aggressive divide-and-conquer to handle even larger datasets. Examples involving partitioning include Bayesian additive regression trees (BART, Chipman et al., 2010, 2012) and local approximate Gaussian processes (LAGP, Gramacy and Apley, 2015; Gramacy et al., 2014). Such predictors are highly accurate, fast, and their divide-and-conquer nature enable vast parallelization. A downside to partition-based schemes, however, is that they result in discontinuous predictive surfaces – pathologically so in the cases of these latter more aggressive schemes. Lack of smoothness is not only aesthetically inferior, it also suggests that predictability is being left on the table when the underlying dynamics are inherently smooth.

In this paper we propose massaging divide-and-conquer GP regression into an aggregation framework in order to smooth over pathological discontinuity, guaranteeing a continuous surface, while at the same time providing a computationally *more* efficient predictor. Our focus is on “smoothing LAGP” although the idea, in principle, can be extended to any predictor furnishing Gaussian predictive equations. Essentially, we propose using the local model’s own predictive (inverse) variance (aka, precision) as a means of patching together and smoothing over functionally independent local predictors. We call the framework PALM, for *precision aggregated local models*. We begin in Section 2 by developing a framework that bridges partition/divide-and-conquer regression with model averaged alternatives, taking the opportunity to connect to recent methods in the literature which leverage such schemes effectively, and those which target smoothing over hard partition boundaries.

Section 3 introduces the PALM framework in generality, but ultimately emphasizes its application with LAGP base models, or “local experts”, and the details required for effective implementation. We illustrate how a limited number of LAGP experts, positioned in a space-filling manner, may be aggregated via precision to yield a fast global predictor which is smooth, and at least as accurate as the ordinary *transductive* (Vapnik, 2013) approach recommended by its creators Gramacy and Apley (2015): apply LAGP exhaustively and independently on each element of a testing set. Section 4 considers how local experts can be allocated sequentially, in a boosting-like framework to regions of the input space/testing set that are harder to predict. Greedy selection allows for a more efficient use of limited computational resources compared to the default space-filling approach. Before concluding with remarks in Section 6, Section 5 augments with empirical work extending the proof-of-concept illustrations provided in earlier sections.

2 Unified partition and aggregation

Partition models, such as based on trees or Voronoi tessellation, divide the data \mathcal{D} geographically into mutually exclusive regions $\mathcal{D}_1, \dots, \mathcal{D}_K$ where $\mathcal{D}_k \cap \mathcal{D}_j = \emptyset$ for all $k \neq j$, and $\cup_{k=1}^K \mathcal{D}_k = \mathcal{D}$. Inference for the splitting structure depends upon a goodness-of-fit criteria paired with choice of model for each \mathcal{D}_i , and a good search scheme. This divide-and-conquer nature has two benefits. One is that fitting smaller models is often cheaper, computationally, than fitting one big model. Nowhere is this more true than with GPs, requiring cubic scaling in flops to decompose large matrices. Another is modeling fidelity. By fitting different models in different parts of the input space, the overall fit is more dynamic than its base version. For GPs, which usually exhibit stationary dynamics, independent modeling and fitting of hyperparameters (θ and η) provides a nonstationary flavor. Nonetheless, the underlying predictor remains within the GP class though an implicit sparse-block covariance structure.

Another way to see this – one which suits our proposed methodology and developments coming shortly – is to represent the partitioned predictor as a weighted average. Suppose we wish to predict at testing site x . Let $w_k(x) = \delta(x \in \mathcal{D}_k)$ indicate whether or not x is in partition element \mathcal{D}_k . Then the partitioned predictor, using GP predictive notation (1) applied separately for each index k via training data $(X_k, Y_k) \in \mathcal{D}_k$, may be represented as

$$\hat{\mu}(x) = \sum_{k=1}^K \hat{\mu}_k(x) w_k(x) \quad \text{and} \quad \hat{\sigma}^2(x) = \sum_{k=1}^K \sum_{j=1}^K \hat{\sigma}_{kj}(x) w_k(x) w_j(x). \quad (2)$$

Above, $\hat{\sigma}_{kj}(x)$ represents the covariance between the predictors in partitions k and j , and $\hat{\sigma}_{kk}(x) \equiv \hat{\sigma}_k^2(x)$. Since the \mathcal{D}_k are mutually exclusive, only one component of the sums in Eq. (2) receive any weight. Each set of predictive equations is itself Gaussian, arising from a GP for $k = 1, \dots, K$, so the weighted sum is also Gaussian and thus a GP.

To illustrate, consider *Herbie's tooth* (Lee et al., 2011). For scalar inputs z , define

$$g(z) = \exp(-(z-1)^2) + \exp(-0.8(z+1)^2) - 0.05 \sin(8(z+0.1)). \quad (3)$$

For inputs x with m coordinates x_1, \dots, x_d , the response is $f(x) = -\prod_{j=1}^d g(x_j)$. Here the default $d = 2$ case is chosen for ease of visualization. Consider a training set composed of a 100×100 uniform grid in $[-2, 2]^2$ and commensurately sized (101×101) , but slightly shifted out-of-sample testing set. In Figure 1, a regular $K = 100$ -element partition is created, and GPs are fit independently to the training data residing in each element of the partition. Full GPs are all but intractable on data of this size, requiring hours to fit on an ordinary workstation.¹ Through divide-and-conquer, fitting each 100-run element in serial takes around two minutes total, and potentially much faster in parallel.

From the figure, a downside to the partition model is readily evident: lack of continuity at boundaries, which at times can be extreme. Attempts to remedy these are not without their limitations. Some seem limited to, or have only been successfully illustrated in, two-dimensional input spaces, and can only guarantee continuity in the mean surface,

¹... using ordinary linear algebra packages

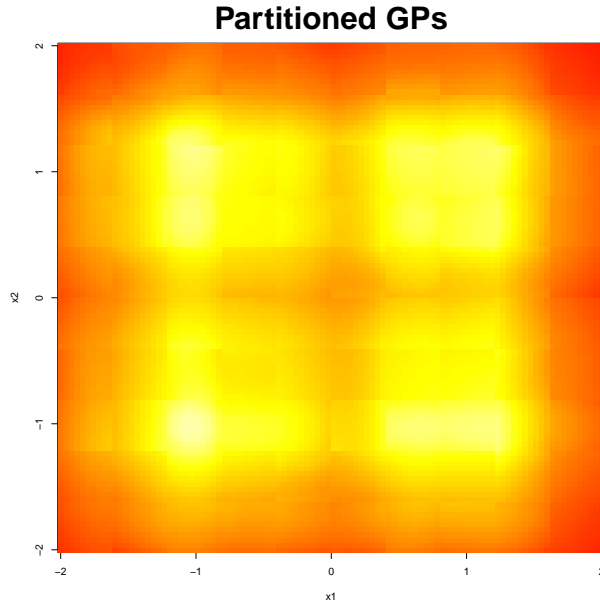


Figure 1: Predictive mean obtained from uniform-partition GP fit to Herbie’s tooth data.

while variances remains discontinuous (Park et al., 2011; Park and Huang, 2016). *Patchwork kriging* (Park and Apley, 2017) can guarantee point-wise continuity at reference locations in both surfaces, but is discontinuous along the full manifold of partition boundaries. As the number of continuity-inducing reference points increases, it will converge to a fully continuous model. Perhaps the biggest downside of approaches attempting to “stitch” boundaries together is that it is not immediately obvious whether resulting predictor is also a GP.

2.1 Extreme partitioning and re-smoothing

A local approximate Gaussian process (LAGP, Gramacy and Apley, 2015) is a purely predictive process that builds a new $n \ll N$ -sized model for each desired predictive location. In this way it is similar to the n -nearest neighbor (NN), although Gramacy and Apley show that when using GP prediction, NNs can be a suboptimal conditioning set. Review of methodological and computational details of LAGP would be a distraction here. See, e.g., Gramacy (2016) for details the `laGP` package for R on CRAN. Intuitively, the method exploits the rapidly decreasing influence of training points on predictive mean and variance as they increase in distance from the predictive location of interest. GP prediction based on a handful of, say $n = 50$ local training sites is fast, highly parallelizable (over a vast predictive set), accurate, and yields a limited nonstationary effect not unlike partition methods. A form of “infinite partitioning” is happening implicitly in the input space \mathcal{D} space from the point of view of the testing set, which makes LAGP an example of *transductive learning* (Vapnik, 2013), as opposed to the usual *inductive* sort. It fits into the form of Eq. (2) when enumerating all K subsets X_N which are of size n and giving only positive weight to those which

are “near” to x . Although that is a daunting enterprise to think about, its implementation is rather straightforward, and compact in terms of storage. Since LAGP finds a new model for each prediction, the storage cost of the model only grows with the size of the original data, instead of $\mathcal{O}(N_k^2)$ like most partition models.

Despite many advantages, LAGP does have drawbacks – many of which may be evident from the narrative above. First, it does not create any permanent model. Each time a new prediction is desired, a new fit must be calculated. This leaves room for similar methods with a permanent model to drastically undercut, trading off space (to store the permanent model) for time. It does not avoid the continuity concerns experienced by other partitioning based schemes. Instead, they are grossly exacerbated: discontinuities are everywhere, although their precise nature may sometimes be difficult to detect with the naked eye.

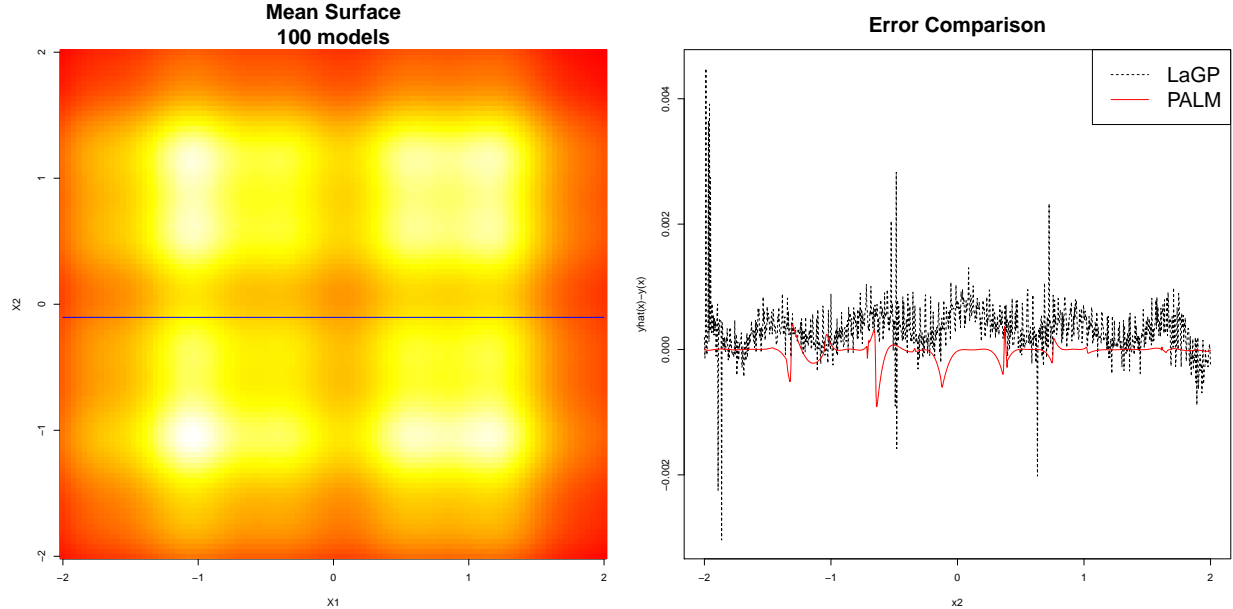


Figure 2: Herbie’s tooth fits: LAGP on left; bias (right) in a slice through LAGP measured against the truth and a PALM competitor.

Figure 2 shows an LAGP fit on Herbie’s tooth data. The left panel mirrors Figure 1, showing a predictive mean surface from LAGP using the defaults in the `laGP` package which uses a neighborhood size of $n = 50$ and greedy local selection by a method called *active learning Cohn* (ALC; Cohn, 1994). The right panel in the figure provides a higher-resolution view via a slice defined by fixing x_2 at -0.104 , as indicated by the horizontal line on the left panel. Rather than showing predictive means on the right, bias $\hat{y}(x) - y(x)$ is plotted instead as a means of “zooming in”. Focus for now on the dashed gray line, corresponding to LAGP. Notice that LAGP’s relationship to the true response, which is itself smooth, is pathologically nonsmooth. Although the overall magnitude of the bias is quite small, at worst 0.006 in absolute value, there are isolated exceedingly poor predictions. Although many biases are much smaller than that, being less than 0.001 in absolute value, there is a

systematic (almost sinusoidal) pattern in these out-of-sample residuals. The red curve, which corresponds to our proposed PALM method, introduced shortly, suggests that both issues – smoothness and predictability left on the table – could be resolved with a modest amount of aggregating, inducing dependence between otherwise functionally independent local fits.

2.2 Model averaging

So far we have only considered boolean weights in Eq. (2). What about more general $w(\cdot)$ satisfying $\sum_{k=1}^K w_k(x) = 1$? The result is a (true) model averaging predictor, representing a potentially smoother alternative to partition models. Such setups have been combined with GPs in order to combat the computational burden of fitting a single large GP (Tresp, 2000). Rather than partitioning, components being averaged can involve overlapping domains or random subsetting of the data, both with and without replacement. A common weighting scheme for these models is $w_k(x) \propto \phi_k(x)$, where $\phi_k(x) \equiv 1/\hat{\sigma}_k^2(x)$ is the predicted precision at x from model k . Such a choice is optimal if the predictors indexed by k are independent and unbiased (Cochran, 1954). The unbiased assumption is often violated, e.g., GPs which are biased toward the prior mean, but precision weighting is nonetheless a default.

A bigger issue is independence. Because model averaging schemes abandon the use of indicator weights, and moreover may use overlapping data subsets, they must deal with multiple model covariance calculations $\sigma_{jk}(x)$ or risk inducing further bias into the meta-predictor (2). Model averaging measures rely on the fact that predictions from component models are independent as long as they have learned the same function. Functional independence of global models can be expressed probabilistically as $P(X_i | X_{-i}, f) = P(X_i | f)$ where f is the global function. While true functional independence cannot be guaranteed, most model averaging schemes are able to show $P(X_i | X_{-i}, f) \approx P(X_i | f)$. With this approximation we can use $\sigma_{jk}(x) = 0$ for all $i \neq j$ since, if they are learning the same function, the separate models are independent. Similar to the partition model, this reduces the variance calculation to $\hat{\sigma}^2(x) = \sum_{k=1}^K \hat{\sigma}_k^2(x) w_k^2(x)$. The quality of this variance estimate is dependent on the approximation to functional independence.

Recombining component models into a unified prediction can work even if the data are not partitioned, as long as independence of the model, given a global function, can be maintained [Chen and Ren (2009)]. The computational complexity for fitting and storage of the model are reduced like in a typical partition model, while prediction is K -fold more work because every predictor is involved for each predictive location x . A drawback, however, is that a common method for justifying functional independence is to have the training sets in each component being quite sparse relative to the global training data. This limits the weighted average’s ability to accurately capture complicated trends, and results in over-smoothing. To illustrate, consider the left panel of Figure 3 which is based on precision averaged global models. The ten thousand point training set is randomly partitioned into 100 models containing 100 points each. Each model’s prediction is weighted by a softmax on precision. Compared to either the left panel of Figure 2 via LAGP, or Figure 1 via partitioning, fidelity is clearly lost. Smoothly varying (e.g., precision) weights guarantee continuity of the surface, but emphasis on local “authority of influence” is starkly absent.

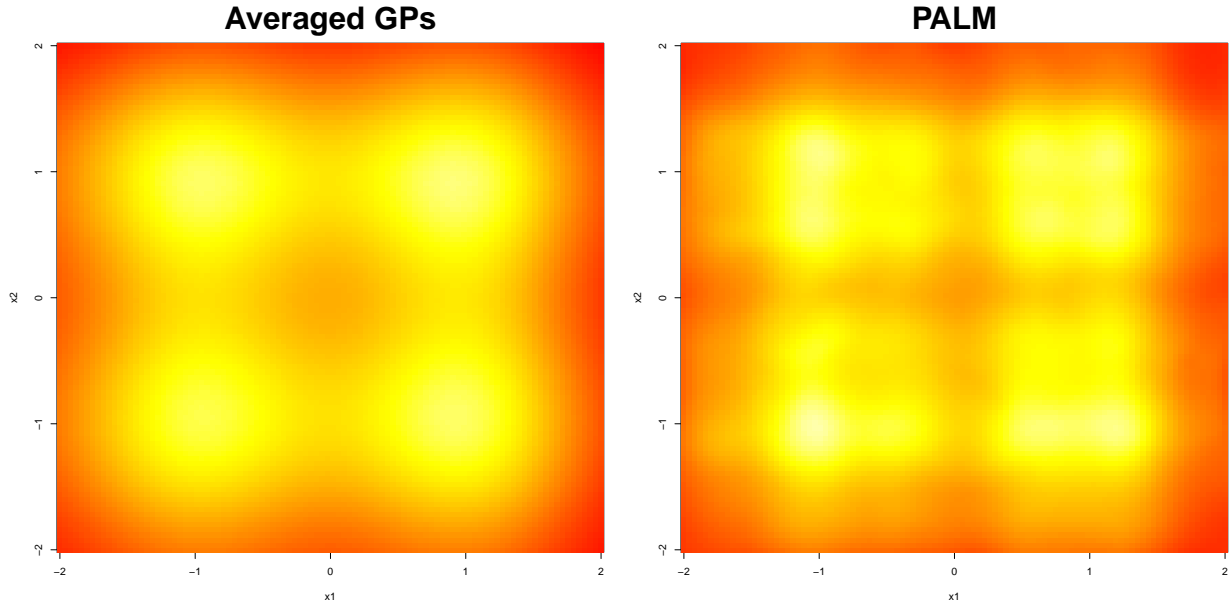


Figure 3: Model averaging (left) and PALM (right) predictions on Herbie’s tooth.

Therein lies the setup for our methodological contribution: PALM (precision aggregated local model). The idea behind PALM is to build locally focused models, as in a partition scheme or LAGP, but which can be smoothly recombined into a global model. The framework introduced in Section 3 momentarily could apply in principle with any local model furnishing smooth predictive means and variances, but our presentation and empirical work favor LAGP. Our goal is to retain the accuracy of an LAGP predictor, but lean on the PALM framework to obtain smoothness and computational gains. Appropriate weighting and accounting for covariance is highly component-model specific and we provide details for LAGP, however similar analogues will be readily apparent. The right panel of Figure 3 serves to whet the appetite. PALM offers a hybrid between predictors shown in earlier figures. Focusing on the slice in the right panel of Figure 2, observe that bias in these out-of-sample residuals is lower, smoother, and has less recognizable pattern than under LAGP.

3 PALM methods

In its most general form, PALM is a method of dynamically weighting predictions from a series of locally accurate models, or *local experts*, to create a coherent global model. Our emphasis is on GP local experts, spaced evenly throughout the input space, but we see no reason why a similar scheme may not be applied more widely. Eq. (2) provides the basic framework; PALM addresses how to choose weights, $w_k(x)$, in order to create smooth and accurate predictions, as well as methods to estimate covariance terms: $\sigma_{kj}(x)$, for $k \neq j$. It is important to reiterate that partitioning schemes (Section 2) are a special case of PALM where one selects $w_k(x) = 1$ for exactly one of $k = 1, \dots, K$, for each x , and zero otherwise.

That weighting eliminates the need to estimate covariance terms $\sigma_{kj}(x)$. On the flip size, a partition model can be converted into a smooth PALM by swapping in smoothly varying weights and estimating between model covariances.

3.1 Warmup: surrogate modeling deterministic evaluations

Local GP approximation, via LAGP, is designed to predict at a specific point x , but in fact that fit offers high quality predictions over a much broader area of the input space. To illustrate, consider the left panel Figure 4 which shows how an LAGP model can offer effective surrogate modeling (prediction and uncertainty quantification) of a sine wave $x \in (3, 7)$ despite being trained only at the “center” value of $x_k = 5$. The objective function is comprised of 1000 equally-spaced points from a sine wave on $[0, 20]$. The training subdesign is derived from default settings in the `laGP` package: starting with six nearest neighbor (NN) points, the ALC criteria is used to greedily select subsequent points before reaching a final size of 50. In the middle panel, the same idea is applied at four other centers spaced evenly throughout the input space. Finally, in the panel on the right, these $\mu_k(x)$ and $\sigma_k^2(x)$, for $k = 1, \dots, K = 5$, are combined with inverse variance weights (2), details coming momentarily, to yield a global predictor which is quite accurate throughout the domain of interest despite a non-uniform density of sampling. The overlapping regions of these five local experts is enough to cover prediction for the entire region.

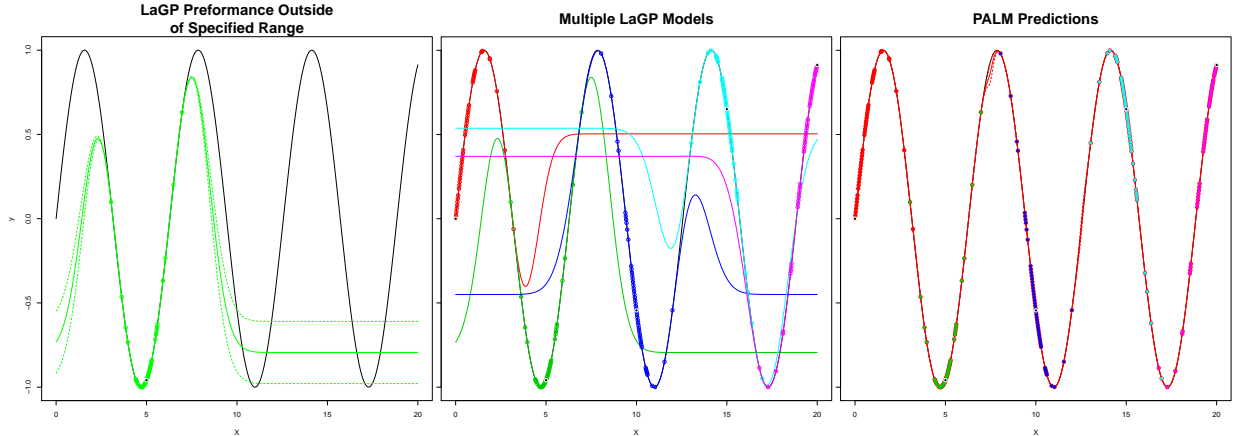


Figure 4: A sine wave modeled by LAGP predictors: alone at one location (left); at five locations (middle); after PALM weighted averaging (right).

A one dimensional example offers convenient visuals – overlapping predictive areas of multiple LAGP and their PALM combination together with an underlying truth – but the same principles hold true for higher dimensions, although visualization is more challenging. The right panel of Figure 3 shows a PALM fit to Herbie’s tooth (3). The training set is based on a 5000 element regular grid, and the “centers” for 100 LAGP local experts (again via `laGP` defaults) were chosen via maximin design² (Johnson et al., 1990). Those local designs

²The maximin criteria was extended to include distance to the boundary in order to build a buffer to

are not shown in the figure, because there would have been too much clutter. However, some are shown later in Section 3.2 when discussing details of the PALM weighting scheme. The testing set was a regular grid of size ten thousand. Full LAGP prediction on those locations takes twelve (core) minutes; our PALM analog takes six seconds.

The right panel of Figure 2 shows a slice through this surface, comparing error from LAGPs trained to every element of that slice of the predictive grid. Notice how the PALM predictor is both more accurate, and also exhibits a smoother bias/higher accuracy compared to the truth. Section 5 presents more examples, but first it makes sense to deliver more detail on how PALM patches together a limited number of local experts to obtain smooth, more accurate prediction, than local experts trained exhaustively in the predictive grid.

3.2 Choosing weights

Choosing a smooth weighting function that simultaneously selects and hybridizes between the right local experts, while maintaining continuity in both mean and variance surfaces, is key to the PALM framework. Inverse variance weighting $w_k(x) = \phi_k(x) / \sum_{\ell=1}^K \phi_\ell(x)$, introduced in Section 2.2, offers a good starting point, combining smoothness and localization according to the local experts’ own judgment. Locally trained GP predictors, e.g., from LAGP, offer an organic and smooth reduction in variance nearby to the local design they are trained upon, and consequently will receive higher weight there. Conversely, higher variance away from their area of expertise will result in lower weight if another expert is commensurately better there. A downside, however, is that GP models are not unbiased – they revert to the prior process, and in particular the `laGP` implementation uses a prior mean of zero. Such bias, then, would become more severe as local GP experts extrapolate.

This means that theory of optimality of inverse-variance weights (Cochran, 1954) does not apply, but coupled with that is perhaps a more practical issue: an inevitable compression of weight in regions of the input space where disparate local experts are equally good/bad. Intuitively, a weight $\phi_k(x)$ should increase nearby a simultaneously shrinking domain of expertise around x , i.e., have weight decreasing elsewhere. However, this cannot happen with a GP expert because predictive variance is also prior reverting. Consequently, adding local experts into PALM, no matter where their local domain of expertise lies, has a flattening or “cooling” effect on individual weights. To combat both issues (bias and cooling) we propose raising precisions to a power p before applying the softmax, i.e., $w_k(x) = \phi_k(x)^p / \sum_{\ell=1}^K \phi_\ell(x)^p$, where p is a function of the number of local experts, K , and the size of the input space, i.e., its dimension d assuming inputs coded to $[0, 1]^d$. In particular, we suggest $p = \log_d K$ as a sensible automatic choice, however another option is to treat p as a tuning parameter which could be optimized on a hold out set.

Figure 5 illustrates the effect of powering up weights. What we see in all panels are the predictive weights given to one LAGP expert’s “center” (open circle) of the PALM used in Figure 3. The figure has been zoomed into the local expert, and the centers of other local experts used in the original model are represented by commensurately sized filled circles.

prevent centers of `laGP` models on the edges of the space, which would effectively clip their area of expertise.

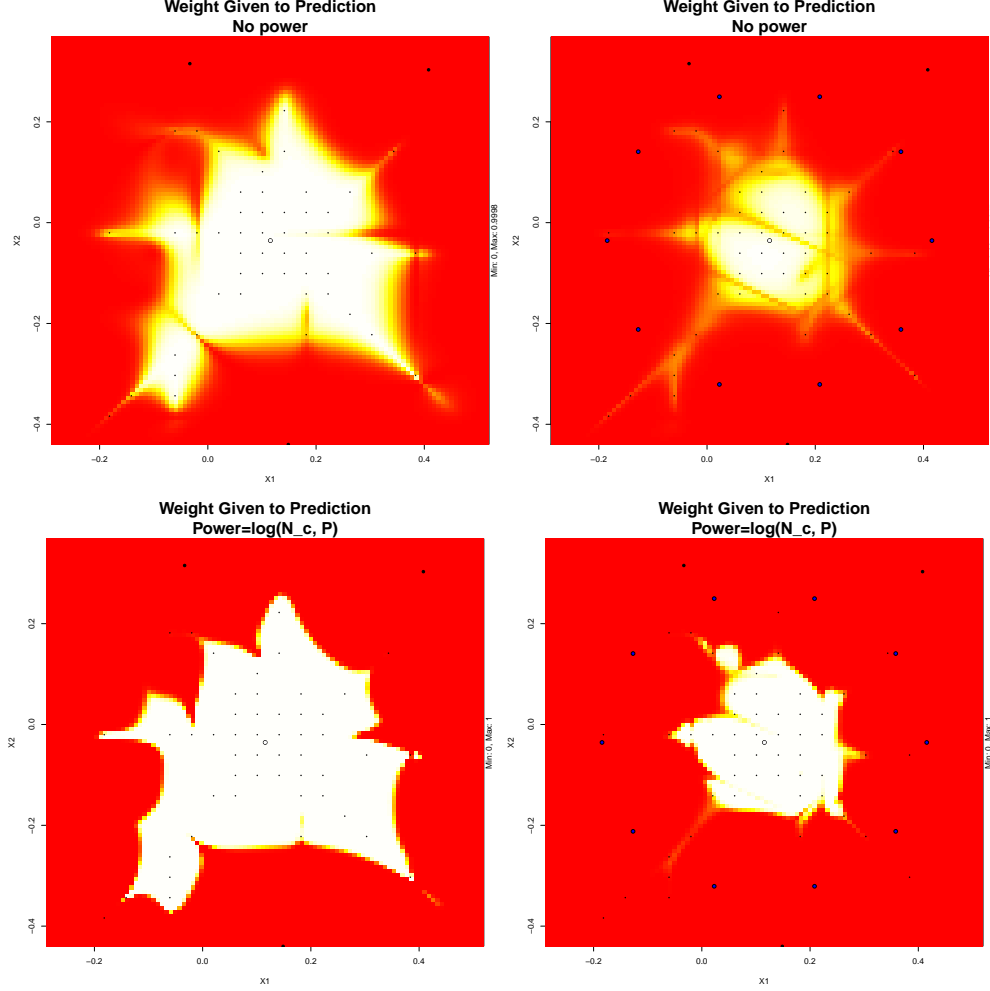


Figure 5: Top left: Weight given to a local expert with $p = 1$, i.e., un-powered. Top right: decrease in weight caused by adding extra models outside of the area of expertise. Bottom left: Local expert weights when powers are used. Bottom right: Added centers outside of the area of expertise do not affect the weight. Large black/blue dots represent other local experts in the PALM, while small dots represent the training inputs X_N .

Smaller dots nearby the open circle indicate the local design selected by LAGP for the open-circle expert. Red colors in the image plot(s) indicate low weight, and lighter/whiter colors indicate high weight. Now consider each panel individually. The top left panel corresponds to softmax precision weights, i.e., $p = 1$, not powering up. For contrast, the bottom left panel uses our recommended power instead, $p = \log_d K$. Observe how powering up has a “heating” effect, making weights more extreme on both ends, leading to fewer yellow/orange and more white/red. In particular, weight is greatly increased in the region nearby the central expert. Otherwise the same of the area with non-trivial (red) weight is largely unchanged.

Now consider the panels on the right in the figure which consider the effect of adding new local experts into the PALM fit. The “centers” of those experts are indicated by larger blue-

filled dots. The top right panel corresponds to no powering up ($p = 1$), and the bottom right one uses $p = \log_d K$. Otherwise everything is the same as on the left; weights correspond to the central expert indicated by the open circle, etc. In the top right, notice that even though the new experts are added largely outside of the original “center’s” area of expertise, the weight for the central expert has gone down, in relative terms (i.e., after re-normalization) everywhere. The non-red area is smaller, and the proportion of yellow is much larger than in any other panel in the figure. Not only has weight gone down within that expert’s domain of expertise but, intriguingly, the presence of the new experts have created streaks of low weight in regions that are very close to those new experts. (The new experts are somehow not experts nearby themselves, albeit in a small volume.) This indicates a lack of ability for pure precision weights to accurately determine which of our experts should be trusted. In the bottom right panel, after appropriately powering up precisions, we see that the same ring of new experts has lowered the weight only inside their own areas of expertise, whereas weight given to the central model remains high in the densely packed region of design points. More experts mean more reactivity in domain of expertise across the input space.

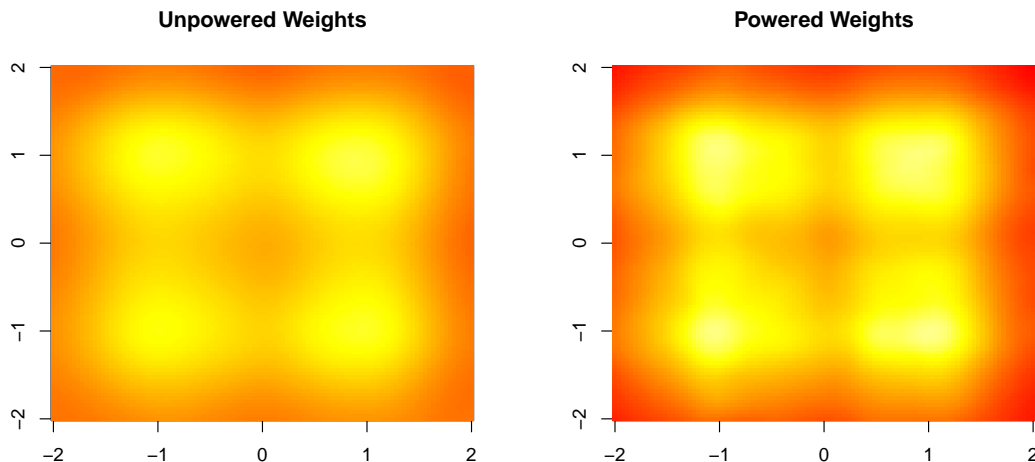


Figure 6: Left: Predictions from a palm using $p = 1$, i.e. pure precision weights. Right: Predictions from the same PALM using $p = \log_2 K$. Local model predictions are unchanged. Only the weight is different.

The effect this has on model prediction is non-trivial. Observe the left panel of Figure 6. Here we see PALM predictions on Herbie’s tooth (following the given experimental details) with pure precision weights, i.e. $p = 1$. Although the rest of the global PALM predictor is performed to the exact specifications laid out here, the model exhibits the same global cooling behavior as the averaged predictor shown above. In the right panel, we apply our recommended $p = \log_d K$ weights, resulting in vastly improved predictive performance.

3.3 Estimating covariance

A major difference between PALM and other model averaging schemes is that we cannot assume functional independence. Other schemes get away with approximate functional independence because each expert k is learning something broad, \hat{f}_k , which is a good approximation to the global function, f . Consequently, globally focused averaging schemes have a relatively constant covariance between models across the input space that authors claim to be low, and tacitly approximate as zero without noticeably ill effect. Locally focused models, on the other hand, can have an extremely high covariance in areas where their domains of expertise overlap, and low elsewhere. An illustration in the LAGP case is coming in Figure 7, a little later in Section 3.4. Because of this, we need a way to estimate the covariance between local experts. Assuming zero covariance will result in underestimating the uncertainty in our predictions (2). A challenge in estimating those covariances is that our local experts assume independence when performing local design and inference. Therefore observing co-variability must transpire as a post-processing step.

Toward estimating those covariances, we begin by decomposing covariance into the product of standard deviations and correlation: $\sigma_{kj}(x) = \sigma_k(x)\sigma_j(x)\rho_{kj}(x)$. The two standard deviations, $\sigma_k(x)$ and $\sigma_j(x)$ are furnished by the predictor from each local expert, so we only need a way to additionally estimate the correlation, ρ_{kj} . Pointwise, for each x and experts j and k , we desire an estimate of the correlation between every pair of models:

$$\rho_{kj}(x) = \text{Corr}(\hat{\mu}_k(x), \hat{\mu}_j(x)) = \frac{\mathbb{E}\{(\hat{\mu}_k(x) - Y(x))(\hat{\mu}_j(x) - Y(x))\}}{\hat{\sigma}_k(x)\hat{\sigma}_j(x)}.$$

For many models, $\rho_{kj}(x)$ may be difficult to estimate, especially when “lazy evaluation” at x is required, i.e., when we don’t yet know where we wish to predict at fitting time. One of the main aims in PALM front-load calculations at training and avoid such expensive calculation at predict time. One way is by estimating a single $\hat{\rho}_{kj}$ for all x , and for all $j, k = 1, \dots, K$, imposing a form of stationarity in correlation over the testing set. Because correlation between models is not constant over the input space, and is only high in the areas where a pair of models have overlapping influence, the non-overlapping space on the set $X_{kj} = X_k \cup X_j$ will artificially drag correlation down. Combined with powered up weights, which helps to ensure that two models will only receive high weight in the area where their influence overlaps, this empirical estimation compounds into a poor estimation of the correlation in exactly the area where the value has the most impact on the model. Again we delay a specific example until Section 3.4.

We find that a suitable stationary value to plug in for $\hat{\rho}_{kj}$ is the maximum value over the input space: $\hat{\rho}_{kj} = \max_x \rho_{kj}(x)$. This formulation, however, becomes increasingly hard to estimate in higher dimension. Moreover $\rho_{kj}(x)$ depends on knowledge of $Y(x)$, a chicken-or-egg-problem at the time of fitting. Thus the final layer of approximation is to replace continuous maximization \max_x with discrete search over data X_{kj} used to train local models j, k . That is, given a class of models for which we can obtain a point-wise estimate of model correlation, $\hat{\rho}_{kj} = \text{Corr}(\hat{\mu}_k(x), \hat{\mu}_j(x))$, we use:

$$\hat{\rho}_{kj} = \max_{x \in X_{kj}} \{\rho(\hat{\mu}_k(x), \hat{\mu}_j(x))\}.$$

Using this formulation, we obtain a high estimate of correlation if either model contains a point in the overlapping area, and a low estimate otherwise. Specific forms for $\rho(\hat{\mu}_k(x), \hat{\mu}_j(x))$ depend on the local expert’s predictive equations; details are given for LAGP in Section 3.4.

We recognize this is an approximation, but our weighting scheme ensures that any inaccuracies would have a minor impact on the uncertainty captured by the PALM predictor. In Eq. (2), observe that the impact on $\text{Var}(x)$, for a single pairing of $k \neq j$, follows

$$\begin{aligned} w_k(x)w_j(x)\hat{\sigma}_k(x)\hat{\sigma}_j(x)\hat{\rho}_{kj} &\propto (\hat{\sigma}_k^{-2}(x))^p (\hat{\sigma}_j^{-2}(x))^p \hat{\sigma}_k(x)\hat{\sigma}_j(x)\hat{\rho}_{kj} \\ &= \hat{\sigma}_k^{-2p+1}(x)\hat{\sigma}_j^{-2p+1}(x)\hat{\rho}_{kj}. \end{aligned}$$

If we pick a form for $\hat{\rho}_{kj}$ which is not too small, i.e., $\hat{\rho}_{kj} \geq \hat{\rho}_{kj}(x)$, we get sensible results from the perspective of conservative estimates of uncertainty. Examine the case where two local models have an overlapping area of extremely high correlation, i.e., $\max_x(\rho_{kj}(x)) \approx 1$, which is the worst case scenario for the disparity between our stationary estimate and reality. When we predict close to the area where $\rho_{kj}(x) = \max(\rho_{kj}(x))$, the true correlation will be close to the maximum and the value we have chosen will benefit the model. As we move away from this area, $(\sigma_k\sigma_j)^{-2p+1}$ decreases faster than the disparity between that max and the true correlation. This squashes the piece of the model variance that is due to this covariance.

3.4 Implementation details

The PALM introduction aimed generic, or agnostic to the choice of expert although LAGP featured as an exemplar. Fixating specifically on that choice, several details must be in place in order to fully operationalize the methodology. Fitting a GP model, local or otherwise, requires selecting hyperparameter settings, such as lengthscales $\theta^k = (\theta_1^{(k)}, \dots, \theta_d^{(k)})$ and scale τ_k^2 . The **laGP** library returns fitted values for these, independently for each predictive location or “center” for PALM. These are designed for predicting at one site only, without knowledge of how PALM intends to utilize those predictors more widely. It may be sensible to revise those estimates in light of the global scope of the wider PALM predictor. Local variation in lengthscales θ_k is sensible, and we have found no need to make adjustments for the PALM setting, except to tailor **laGP**’s prior to discourage extremely large lengthscales. Assuming we have no knowledge of the global lengthscale, we can find a reasonable estimate by building several global GP models using small random subsets of the data, and selecting the largest maximum likelihood estimate from among them to be the maximum value that each **laGP** may choose. Local experts may then adjust downward as necessary.

Scale τ_k^2 requires a more careful treatment, however, since it determines the amplitude of variability in the predictor (1). When trained on a local design, $\hat{\tau}_k^2$ could only reflect the scale of the local training design. When applied globally through predictive equations, this could be a mismatch to a much broader global scale, and thus result in extreme inaccuracy especially in terms of predictive variance. This is particularly important since predictive variance is used to determine the weight of local models upon recombination through the softmax. Therefore, instead of estimating a separate amplitude for every model, we prefer to leverage information from all local experts to enforce a single hyperparameter value. In

other words, we are building in an assumption of global stationarity in scale. One option here which is attractive theoretically is to perform inference for a global τ^2 by maximum likelihood, where the likelihood is comprised of a product of K MVN densities whose means and covariances follow K applications of Eq. (1), one for each local expert. In practice, however, this is intractable for even modestly sized training sets N , owing to the requisite cubic decomposition of $N \times N$ matrices. Instead, we prefer the following idea.

Hyperparameter τ^2 doubles as amplitude and asymptotic variance $\tau^2(1 + \eta)$ of a GP model, measured as the correlation to training data X_N decays to zero. For now, take nugget as jitter for interpolation of simulations observed without noise, $\eta = \varepsilon$, however details for the noisy case will be provided momentarily. Reverse engineering a bit then, consider measuring that asymptotic variance through the PALM predictor instead. Below s^2 represents the empirical variance of the response vector, y , via simple residual sum of squares around the average \bar{y} . The plan is to use that estimate to define what the asymptotic variance of the final PALM fit should be. Let quantity τ_{PALM}^2 represent the effective amplitude parameter of the full PALM, while τ^2 is the amplitude we use to fit the local experts in order to achieve the correct extrapolation properties.

What we want is for the asymptotic amplitude of our PALM fit to be equal to the measured amplitude of the training data. In other words, we want $\tau_{\text{PALM}}^2(1 + \eta) = s^2(1 + \eta)$. In order to achieve this, begin with the formula for variance from the PALM fit (2)

$$\hat{\sigma}^2(x) = \sum_{k=1}^K \sum_{j=1}^K w_k(x) w_j(x) \hat{\rho}_{kj} \hat{\sigma}_k(x) \hat{\sigma}_j(x),$$

with covariance estimates (correlation and standard deviations) plugged in. It is important to remark that the weight function, $w_k(x)$ depends on the GP correlation function between the data used to train model k , and the predictive location x as $k_k(X_k, x)$ through the GP variance function, $\hat{\sigma}_k^2(x) = \tau^2(1 + \eta - k_k^\top(x) K_k^{-1} k_k(x))$. As predictive location x moves away from the corpus of data used to train PALM experts (a subset of the full training data), each of the GP correlation functions approach 0. This causes the weight each PALM “center” receives as they extrapolate to be approximately equal, i.e., uniform. Consequently, we may replace those weight functions in the double sum above with $1/K$ where K is the total number of experts in the full PALM.

$$\text{As } \lim_{k(X_k, x) \rightarrow 0} w_k(X) = \frac{1}{K}. \quad \text{we have that } \hat{\sigma}^2(x) \rightarrow \frac{1}{K^2} \sum_{k=1}^K \sum_{j=1}^K \rho_{kj} \hat{\sigma}_k(x) \hat{\sigma}_j(x).$$

We may further use the limit of the GP correlation function to remove $\hat{\sigma}_k(x)$ from the double sum. As each $k_k^\top(x) K_k^{-1} k_k(x)$ approaches 0, $\hat{\sigma}_k^2(x) \rightarrow \tau^2(1 + \eta)$, simplifying to

$$\hat{\sigma}^2(x) \rightarrow \tau^2(1 + \eta) \frac{1}{K^2} \sum_{k=1}^K \sum_{j=1}^K \rho_{kj}.$$

Finally, remembering that we want to pin this value to a reasonable amplitude based on the variance of the observed response vector, we can solve for τ^2 , the amplitude that should be plugged into each individual local expert. Specifically,

$$s^2(1 + \eta) = \tau^2(1 + \eta) \frac{1}{K^2} \sum_{k=1}^K \sum_{j=1}^K \rho_{kj}, \quad \text{giving} \quad \tau^2 = s^2 \frac{K^2}{\sum \sum \rho_{kj}}.$$

The final ingredient above, circling back the generic discussion in Section 3.3, is estimating ρ_{kj} , the correlation between LAGP experts. Define the *predictive kernel* of each expert j to be the matrix wise correlation between each point in the model, and predictive location x :

$$k_j(X_j, x)^\top K_j k_j(X_k, x). \quad (4)$$

For each pair of models kj , we may find the kernel when using one model to predict the other, and visa versa. A sensible estimate for between-expert empirical correlation is the maximum value found in the combined vector of predictive kernels. Let $\rho_{kj}^\ell = k_k(x_\ell) K_k^{-1} k_k(x_\ell)$, where ℓ indexes each $x_\ell \in X_j$. Then, take

$$\hat{\rho}_{kj} = \max \left(\rho_{kj}^1, \rho_{kj}^2, \dots, \rho_{ij}^{|X_j|}, \rho_{jk}^1, \rho_{jk}^2, \dots, \rho_{jk}^{|X_j|} \right). \quad (5)$$

This kernel based correlation estimate (4) is bounded on $[0, 1]$, and is highly positive for models that are close to each other, while approaching zero for those that are separated. To illustrate this, Figure 7 displays two local experts used to model the sine wave from Figure 4. Note that these are not the same models from above, but have been moved closer together to ensure they overlap for dramatic effect. Solid lines represent the GP correlation (4) between each model and every point along the wave. Dashed lines show the weight that each model receives in predicting along the function. We have put the points used to build local experts along the correlation line for the opposite model, and colored the maximum point (which is used as the value for $\hat{\rho}_{kj}$) in light blue. Notice the value we choose for $\hat{\rho}_{jk}$ following Eq. 5, shown as a blue diamond for easy visibility, is very close to 1, which is accurate for the area of weight overlap. This value may not be accurate for the entire input space, but one of the models receives nearly zero weight for all egregious areas. Using estimates $\hat{\rho}_{kj}$ we calculate predictive variance at any new point using

$$\hat{\sigma}^2(x) = (\vec{w}(x) * \vec{\sigma}(x))^\top \hat{\rho} (\vec{w}(x) * \vec{\sigma}(x))$$

where $\vec{w}(x) = (w_1(x), w_2(x), \dots, w_K(x))$, $\vec{\sigma}(x) = \{\hat{\sigma}_1(x), \hat{\sigma}_2(x), \dots, \hat{\sigma}_K(x)\}$, “*” is a component wise, Hadamard product, and $\hat{\rho}$ is the matrix containing empirical correlation values.

Regression for noisy data

The major difference between a deterministic GP model and the stochastic version is the incorporation of a nontrivial nugget value, η , which breaks interpolation for smoothing, allowing for variance at training data points. The **laGP** function can return an estimated

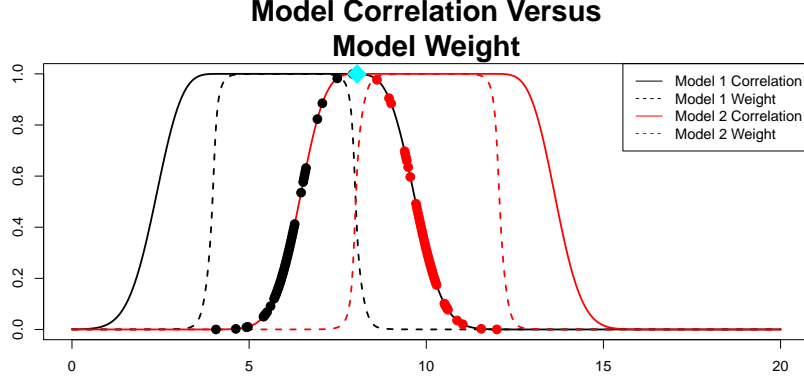


Figure 7: The correlation chosen between two local experts overlaid with the weight they receive in the model. The estimated correlation is shown as a blue diamond for visibility.

nugget for each local expert, obtained by maximum likelihood. This ignores that we intend to use the this local expert as part of a unified model. It’s also overkill because separate nuggets mean heteroskeasticity (i.e., input-dependent noise Goldberg et al., 1998; Binois et al., 2018), and thus unnecessary estimation risk. We instead desire a pooling of estimated variance, toward a single nugget for the entire global surface, although return to the potential for greater flexibility in our discussion in Section 6.

One option is maximum likelihood, though the sum of normal log densities with mean and variance defined by (2). Unfortunately, we have not found this to be computationally tractable. Instead, we prefer a moment-based approach. Recognizing that the minimum possible variance is $\tau^2\eta$, we select η such that this minimum meets our estimate of the variance at a specific point. For each local expert, we find $\widehat{\text{mse}}_k = \frac{1}{|X_k|} \sum_{i=1}^{|X_k|} (\hat{y}_i^{(k)} - y_i^{(k)})^2$, where $\hat{y}_i^{(k)}$ and $y_i^{(k)}$ are fitted values from model k and observed training values, respectively. We then use the empirical $\widehat{\text{mse}} = \sum_k \widehat{\text{mse}}_k / N_k$ as our estimate of the minimum variance for a model, \hat{s}^2 . This leads to the selection of $\hat{\eta} = \hat{s}^2 / \hat{\tau}^2$ as the unified nugget for all experts.

3.5 Illustration

A broader suite of empirical benchmarking results is provided in Section 5. However, before moving to sequential selection of experts in Section 4, we pause briefly here to provide some initial proof-of-concept results in this simpler, static setting. Here, and later in Section 5, we contrast model quality and performance along several key metrics. First, to compare quality of predictions, we measure the out-of-sample root mean squared prediction error (RMSE). For N' testing data examples,

$$\text{RMSE} = \sqrt{\frac{1}{N'} \sum_{i=1}^{N'} (y_i - \mu(x_i))^2}.$$

Second, we consider the proper scoring rule introduced by Eq. (27) in Gneiting and Raftery (2007), which is a reduced form of the scoring rule utilizing two moments – a special case of Eq. (25) from that same paper.

$$\text{score}(\mu(X), y) = -\frac{1}{N'} \sum_{i=1}^{N'} \frac{(y_i - \mu(x_i))^2}{\sigma^2(x_i)} - \log(\sigma^2(x_i))$$

Notice how score offers good balance of predictive accuracy through $(y_i - \mu(x_i))^2$, and uncertainty quantification through $\sigma^2(x_i)$. We expect that whatever we might lose in predictive accuracy from LAGP can be made up by leveraging global information for proper variance estimates. Lastly, we note predictive time. This metric is the main catalyst for developing the PALM methodology, and we would expect a massive advantage over other methods with a similar predictive accuracy.

Table 1 summarizes the results of a simulation study comparing PALM and LAGP on these important metrics, including time per prediction in seconds. We fit a PALM with $K = 100$ space-filling centers, each with the default `laGP` settings, to Herbie’s Tooth (3) generated on an $N = 100 \times 100$ grid in 2d. Training responses are sampled under a standard zero-mean Gaussian with $\text{sd} = 0.05$. The testing set is generated from the same function on a 101×101 grid, deliberately spaced to miss the training data locations. Observe that RMSE and score are practically identical between the two predictors. Even for a small PALM (only 100 local models, utilizing fewer than 5000 of the 10000 training sites), we have achieved comparable results to LAGP, which utilizes every training data location, while predicting in a thirtieth of the time.

	RMSE	Score	Time
LAGP	0.0515	4.9062	0.0628
PALM	0.0525	4.8887	0.0021

Table 1: Mean RMSE, score, and predictive time per point on Herbie’s tooth. PALM had an average model build time of 93 seconds, for a 114 seconds to predict 9801 points.

If we increase the size of the PALM, we can match the performance of LAGP while maintaining predictive advantage. Figure 8 shows the predictive capability of PALMs of various sizes versus that of LAGP. To accommodate predictors trained on larger data sets, we increase the size of the training data set to 40 thousand on a $N = 200 \times 200$ grid, and similarly expanded the testing set is on a 199×199 grid (size 39601), both otherwise generated as described above. The black line in the right panel of the figure represents the score of PALMs with the number of space-filling centers indicated on the x -axis. On the right, total predictive time is plotted for the same fits. LAGP is in red on both plots. Note that the line is horizontal because LAGP builds a separate model for each prediction, and thus does not have an increasing size component. Of particular interest is PALM’s predictive time, shown in the right panel, which indicates a very slow increase. Despite diminishing returns in score as model complexity increases, a larger PALM provides generally better performance in terms of cost–benefit trade-off relative to raw LAGP.

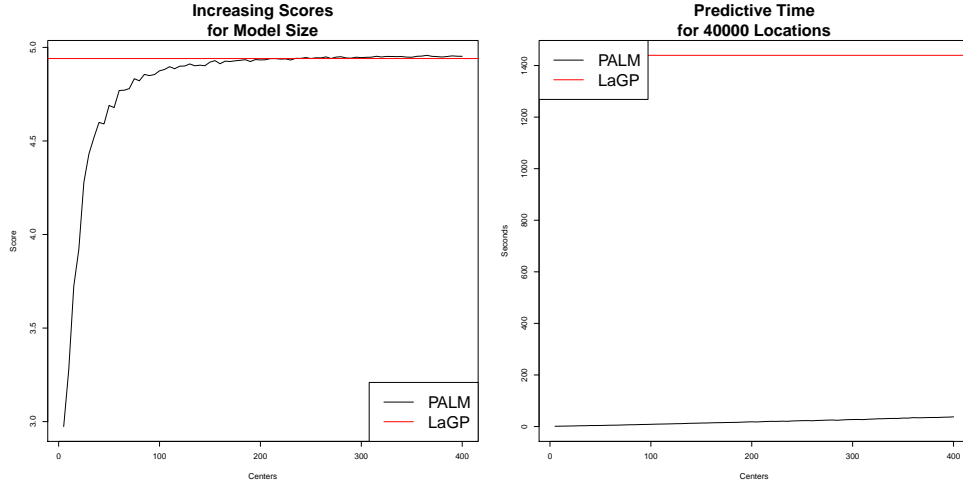


Figure 8: Score (left) and predictive time (right) for increasingly large PALM v. LAGP.

For deterministic data, accurate variance representation allows for PALM to perform much better than LAGP with a vastly improved predictive time. Figure 9 shows the performance of both models on a Herbie’s tooth (3), generated here with a standard deviation of 0. The training and test sizes, and design locations remain the same as above. The plot should be read the same way as Figure 8. Notice that PALM matches and surpasses the performance of laGP while maintaining a large advantage in time.

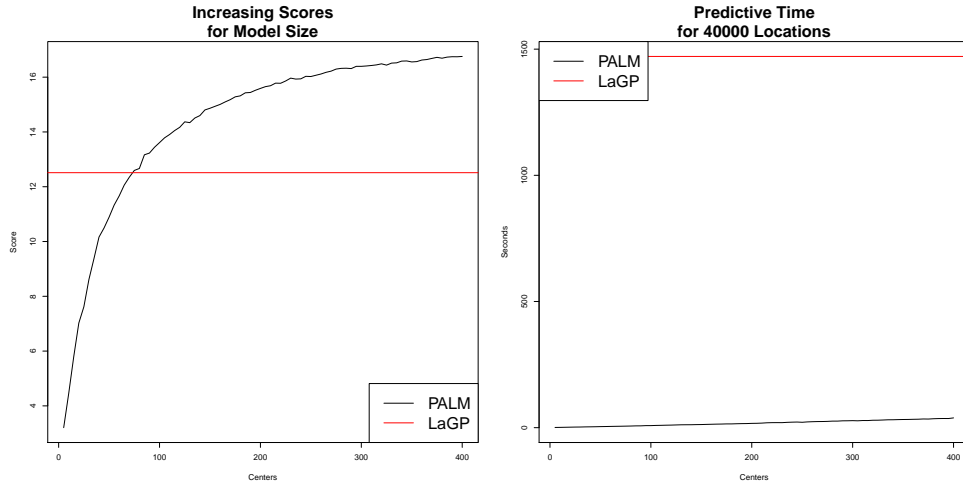


Figure 9: Analog of Figure 8 on deterministic Herbie’s tooth.

4 Sequential Selection

Until this point we have utilized equally-spaced experts (or LAGP centers) when PALM fitting. While this suffices for low-dimensional examples exhibiting highly regular (i.e., sta-

tionary) dynamics, bigger problems and more complex (e.g., nonstationary) response surfaces may benefit an uneven spread of computational resources to accurately capture the global surface. Consider the 2d exponential function from Gramacy and Lee (2008).

$$f(x) = x_1 \exp\{-x_1^2 - x_2^2\} \quad (6)$$

Exponential decay means that the response surface is essentially zero everywhere except near the origin. Although dynamics are smooth, bumps near the origin create subtle nonstationarity. Capturing both bumpy and flat regions, we take inputs in $[-2, 6]^2$.

In Figure 10, we have intentionally limited the number of local experts to illustrate how their uneven distribution may improve global accuracy. In the left panel, 16 experts have been assigned to fill out the space. Observe that only one local expert center resides in the interesting region near the origin. In the right panel, four points have been assigned to represent the interesting area before the other 12 are filled in by a space filling scheme in the flat area of the function. This adjustment in scheme results in much better coverage of the more complicated area, and an overall reduction in error, as we shall quantify in more detail in due course. For now, notice that the right panel exhibits greater relative isotropy compared to the left panel. Looking at Eq. (6), radial decay is evident in $x_1 \times x_2$ space.

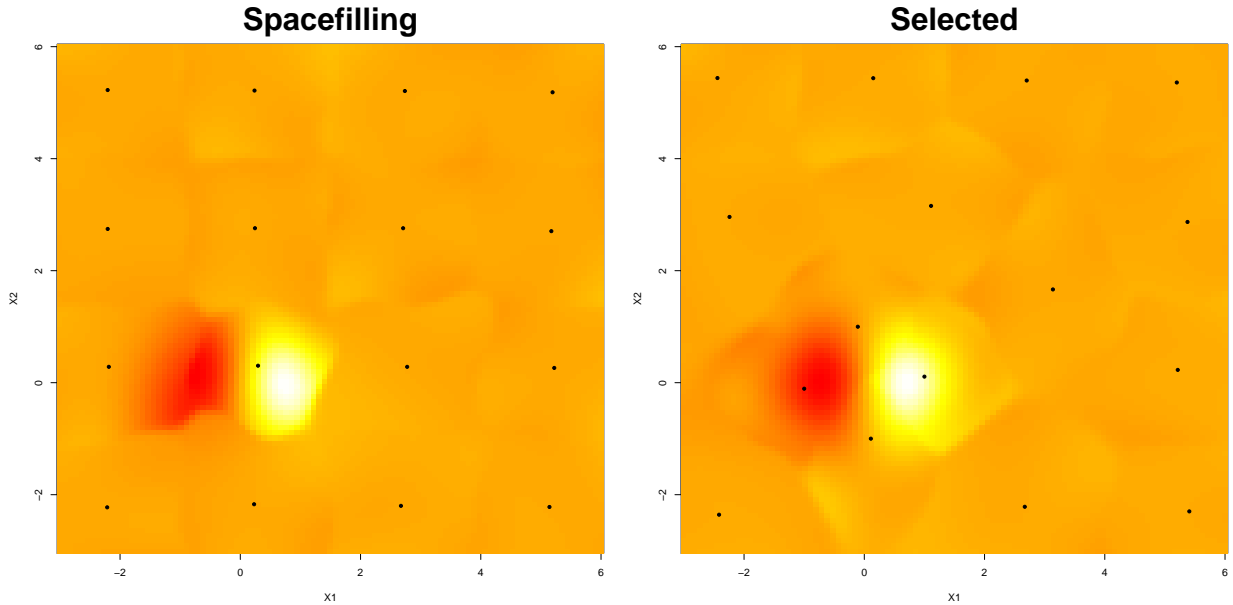


Figure 10: Two different schemes for location of local experts: gridded (left) and re-focused on the interesting region (right).

4.1 Greedy selection of PALM centers

Allocation of experts/centers in the simple case above is rather straightforward if one has prior knowledge of the surface, which is in general unrealistic. For most functions we will

not have prior knowledge of hard to compute areas or, in more than 2 dimensions, an ability to directly visualize them. For similar reasons, optimizing the locations of all centers simultaneously could be challenging. Instead, we find it advantageous to proceed sequentially. Given an existing PALM, we consider optimization of the selection of one additional local expert. Such a greedy strategy, targeting areas of the input space demonstrating the greatest benefit to expanded modeling fidelity, mirrors LAGP’s scheme for choosing local design sites sequentially, e.g., using a variance reduction scheme (i.e., ALC).

In our context of greedy center selection we have the luxury of measuring out-of-sample accuracy directly, rather than relying on a model-based deduction of predictive uncertainty (ALC). Namely, we can calculate residuals between predicted and actual responses under the PALM fit. Therefore, our development of criteria for greedily selecting new centers focuses on identifying areas of the input space suffering from large such (absolute) residuals. Specifically we deploy k -means Lloyd (1982) on pairs (x, r) , where $r = |y - \hat{y}|$ and x is the input location(s) of those y -values, in order to find clusters of high residuals where additional centers may be most helpful at increasing accuracy. In practice we find it helpful to scale those absolute residuals to be commensurate in size with the coding of inputs x in order to encourage the algorithm to form spatially contiguous clusters. A PALM with K centers should have on the order of K “local maxima” for poorly predicted areas, so in practice we set the number of k -means clusters to be equal to the number of local experts in the model. We denote the k -means algorithm, applied to a data set, X_N , with k clusters as $\text{kmeans}(X_N, k)$. Next, we identify the cluster with highest average residual, place a bounding box around that geographical region of the input space, and perform a local numerical optimization in order to fine-tune the location of the new center.

Our choice of that final criteria for local optimization is nuanced. Ideally we would maximize score or aggregated absolute residuals. However, as a function of LAGP sub-design(s), both are discontinuous – score pathologically so – thwarting off-loading of optimization to simple library-based schemes. Instead, we leverage an empirical observation that good predictive areas tend to be far away (in the input space) from other local models in hard-to-predict areas. In other words, space-filling in a high residual region – e.g., as selected by k -means – offers a decent surrogate for score or residual-optimizing. Figure 11 shows the intuition for this idea. The horizontal red line represents the score of a PALM designed to fit a grid of 10,000 equally-spaced points along a sine wave with centers located at the vertical blue lines. The jagged black line is the score for a new center placed at that spot on the x -axis. The green line is the absolute residual at that point in the existing PALM.

Observe in the figure that if we were to select a local area that had high absolute error, and then subsequently choose a space filling location/midpoint within that space, it would correspond with a high score/high absolute residual area of the input space. Also note that the only center locations which make the PALM worse than the existing model are the locations of the current centers. Therefore we have designed our greedy scheme to choose a new center, c , such that $c = \arg\max_{c \in B} \min_{z \in C} \|c - z\|$ where c is the location of the new center to be added, B is the bounding box around the poorly predicted cluster of residuals, and C is the matrix containing the locations of centers already in the model appended by

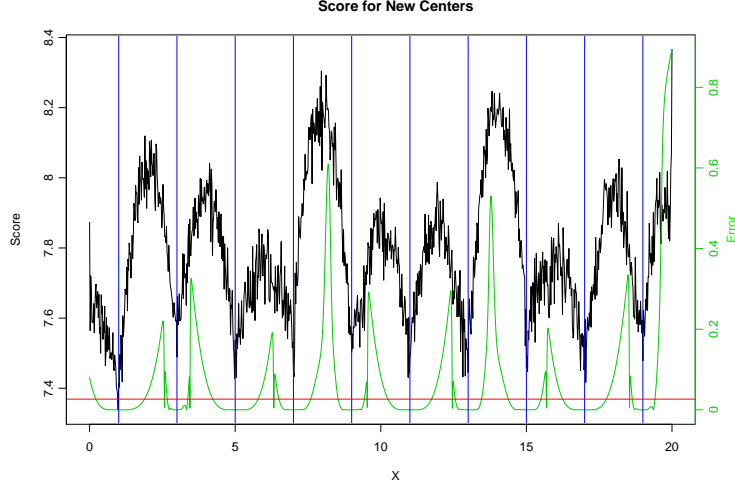


Figure 11: Score for potential new local expert placement against the absolute error of the existing model. The horizontal red line represents the score of an existing model, while the black line represents the score for a model updated with a center located at that spot along the number line. The (right) “error” axis indicates the absolute error for predictions using the existing model at that location.

Require: existing PALM model with N local experts, input locations X , response vector y , matrix of existing center locations C

1: $\hat{y} \leftarrow \text{predict}(\text{PALM}, X)$	{Predict on the known input locations}
2: $r \leftarrow y - \hat{y} $	{compute absolute residuals}
3: $R \leftarrow \text{bind}(X, r)$	{Combine input space and residuals}
4: $K \leftarrow \text{kmeans}(R, N)$	{Form into k contiguous clusters}
5: $X_k \leftarrow K[\bar{r} = \max(\bar{r}), -r]$	{Find the cluster with high residuals}
6: $B \leftarrow \text{apply}(X_k, \text{range})$	{Compute the bounding box in the input space}
7: for i in 1 to M_s do	
8: $c_{\text{start}} \sim \text{uniform}(B)$	{Uniformly generate starting point}
9: $s_i \leftarrow \text{optim}_{c c_{\text{start}} \in B} \min \ c - z\ _{z \in C}$	{Optimize from the random start}
10: end for	
11: $c_{\text{new}} \leftarrow \text{argmax}_{s \in S} \min \ s - z\ _{z \in C}$	{Find overall best solution}
12: $\text{PALM} \leftarrow \text{PALM} \cup \text{laGP}(c_{\text{new}})$	{Append the PALM with a new laGP}
13: $C \leftarrow C \cup c_{\text{new}}$	{Add in the new center location}

Algorithm 1: Computing the location of one more center given an existing PALM fit.

the corners of the bounding box. This “maximin” criterion is a continuous function which is easily optimized with library methods such as `optim` in R, although within the bounding box there may be several local maxima. To combat this we engage a randomized multi-start scheme. Finally, build an LAGP forming local expert for the PALM centered at the solution. For concreteness, the complete sequential PALM center-updating algorithm, with M_s being

the number of multi-start maximin attempts is summarized in Algorithm 1,

4.2 Illustration

To get familiar with this greedy scheme, we provide a visualization and empirical comparison on the Gramacy and Lee function (6). A regular grid of $N = 40000$ training data pairs is created deterministically. We begin with a PALM composed of a small space filling design with $K = 5$ centers. The absolute residuals from this model are seen in the top left of Figure 12. None of the points have been placed within the area of interest, resulting in

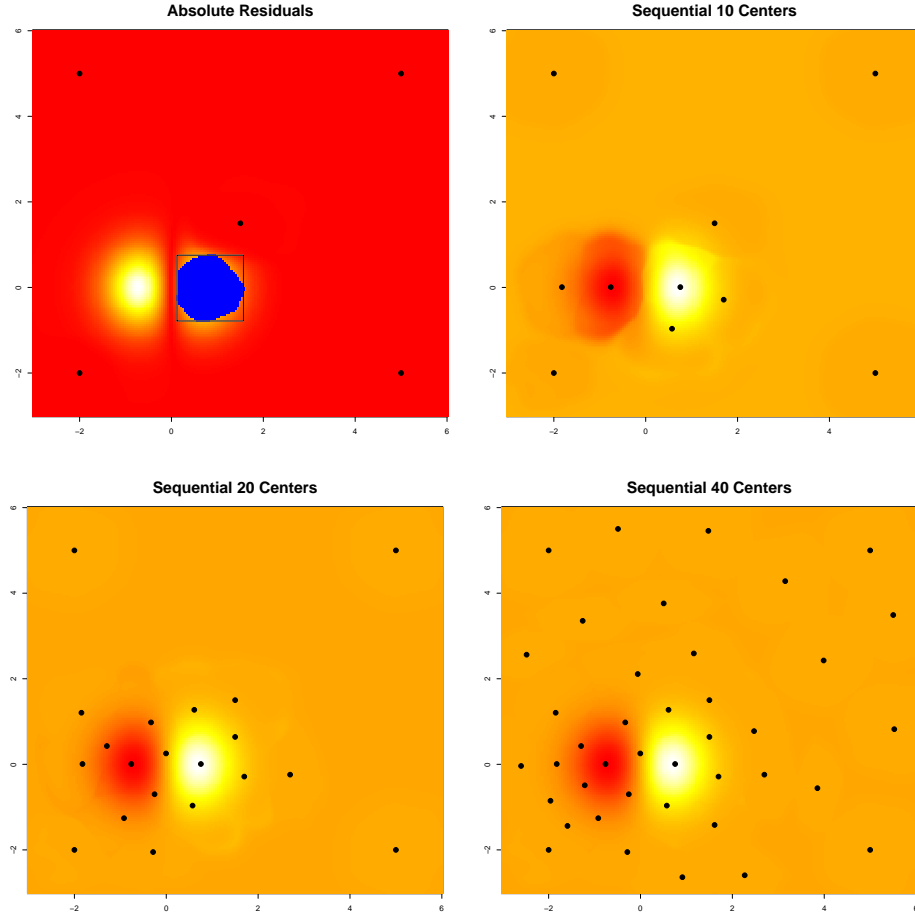


Figure 12: An illustration of the sequential selection process. The top left panel has 5 space filling centers. The top right, bottom left, and bottom right follow our sequential algorithm to achieve total sizes of 10, 20, and 40 centers respectively

two high areas surrounded by relative flatness. The k-means algorithm selects one area of high residuals, shown here in blue, and a bounding box is drawn around them. In this case, where there are no existing centers inside the box, the new expert will be designed to predict

exactly the middle of the high residual area. To the right, we have placed five more centers, one at a time following the greedy scheme outlined in Algorithm 1. Observe that all have been chosen in the difficult area of the input space, near the origin. The bottom left panel shows a further 10 sequentially selected centers. Now our greedy selector is starting to form a good picture of the interesting region and is exploring putting centers around the edges to determine where the function returns to a flat state. By the time we reach $K = 40$ centers, in the bottom right, the PALM has well described the whole region and is selecting additional centers in a space filling fashion around the interesting region as well as elsewhere.

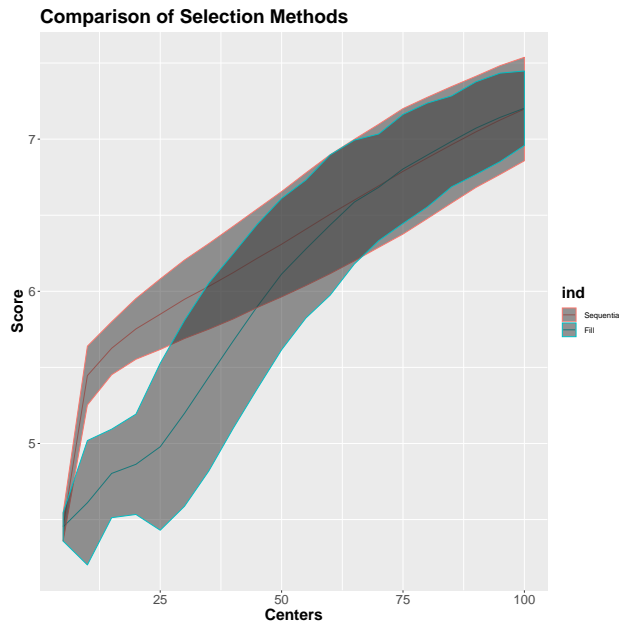


Figure 13: The score of models of various sizes when space filling, or applying a sequential selection algorithm on the Gramacy and Lee function.

Figure 13 shows how sequentially selecting can potentially drastically improve PALM fits, but will do no worse than a space filling baseline. This time we generated commensurately-sized data (6) with noise ($\text{sd} = 0.01$). For 100 such randomly generated data sets, PALMs were built with 5 to 100 centers incrementing by 5 in a space-filling fashion. The out-of-sample performance of this space-filling comparator is indicated by the blue lines in the figure. The red line, however, represents the above greedy/sequential selection scheme. An initial/seed spacefilling model of size 5 was built, and all subsequent centers were added by greedy selection following Algorithm 1. Notice that the sequential scheme has a sharp spike for smaller models, but levels out to match the space filling models in the long run. This represents a early concentration of centers around the “interesting area” near the origin before the sequential scheme starts filling in the rest of the space.

In general, if there is no prior knowledge of the interesting areas of a function, sequential selection of center locations will provide a potential boost in model accuracy by concentrating resources in the active subspace of the model. When the resources allocated are enough to

describe the entire surface well, a sequentially selected model will match the performance of a spacefilling scheme. By front loading calculation on determining center locations, the overall performance of a PALM fit can be improved.

5 Empirical work

To further test the viability of the PALM framework, passages below describe its application on more complicated data sets than the illustrative examples given thus far. First we shall demonstrate the effectiveness of our method on a real data example from a spatial data forecasting competition, allowing comparisons to be drawn to a variety of other GP-based and related large-scale smoothing methods. Then we show a comparison of space filling versus sequentially selected center designs on a classic three dimensional test function.

5.1 Satellite Data

In Heaton et al. (2019), thirteen state-of-the-art spatial smoothing methods, many based on GPs, were compared out-of-sample on satellite temperature data under a variety of performance metrics. This provides a real data example over which we can benchmark PALM to modern competitors. Several were reviewed in Sections 1–2, including a variation on LAGP. All methods and their implementation can be found in the repository linked below.

<https://github.com/finnlindgren/heatoncomparison>

The dataset consists of land surface temperatures measured remotely over 150 thousand locations selected from a grid, however 1691 record “missing” (or NA) values, leaving 148,309. See the left panel of Figure 14. Heaton et al. partitioned these data into training and testing sets; see the right panel. The training data represents a large portion of the full data, at 105,569 sites, but has substantial swaths of sparse or entirely missing coverage. In the exercise reported in that paper, the testing set was completely hidden from competitors.

We built two variations on PALM to add into the mix. The first uses $K = 2000$ LAGP experts built in the usual fashion: to directly predict the response. Centers for those models are selected as a space-filling subset of the desired prediction locations – the testing set – which focuses the majority of our computational power on sites where the predictor will be scored. In this way, the application of PALM here is similar to the transductive spirit of LAGP (Vapnik, 2013), where learning is focused on locations where predictions will be tested. It should be noted that the resulting PALM is not appropriate to describe the entire surface, but a prediction-focused model is better suited to the uniquely extrapolative nature task at hand. The second PALM variation is fit in two stages: first a global GP model is trained to a 1,000-sized sub-sample of the data points; then a PALM is fit to residuals from that global subset GP using the same 2,000 central locations from the first PALM variation.

Table 2 shows a comparison to the methods from the Heaton et al. bakeoff on the same metrics given in the original paper: mean absolute error (MAE), root mean squared error (RMSE), continuous ranked probability score (CRPS; see Section 4.2 of Gneiting and

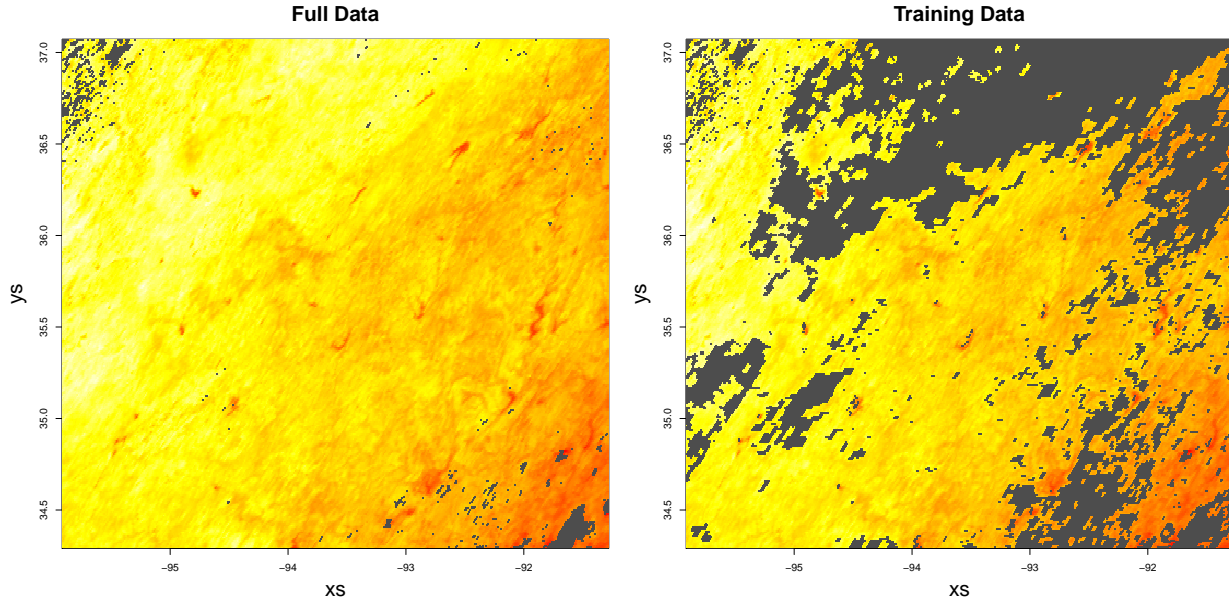


Figure 14: Left: full satellite temperature data set. The few missing values are displayed in gray. Right: dataset subset used for training. Much more data is left intentionally missing.

Raftery (2007)), interval score (INT; see Section 6.2 of Gneiting and Raftery (2007)), prediction interval coverage (CVG), and run time (minutes). Additionally we added a proper scoring rule (i.e., Eq. (27) from Gneiting and Raftery, 2007) metric to enable a more direct comparison to LAGP connecting to other criteria and comparison made throughout this article. Notice that our PALM was run on just one core, whereas several of the other methods leverage symmetric multi-core parallelization. As discussed previously, and again in Section 6, PALM is easily parallelizable. Speculatively, our method could be 40 times faster if given access to the same number of cores as, say, LAGP.

Observe in the table that PALM is performing favorably compared to other state-of-the-art methods. Using only one core, we are able to make predictions faster than most other models, and ones which are competitive on accuracy (i.e., via MAE and RMSE) of the best of the others. In this example, the “Global+PALM” method does slightly better on all predictive measurements. This could be due to the extrapolatory nature of the problem at hand. With the majority of the computational power focused on an area with relatively little observed data, some estimate of a global trend improves the overall prediction quality.

While PALM has a speed advantage over many competitors in the group, it is in the middle of the pack for most predictive metrics. Perhaps this could be improved by increasing the number of local experts, K at the expense of time. Also note that PALM, in its conception, is designed to leverage the wide area of accuracy of individual LAGP models across the input data (i.e. not to cover large areas of extrapolation). Despite this the “off the shelf” version of PALM is still competitive with state of the art methods. We have not explored much the effects of inverse variance weighting in extrapolation, or the performance

	MAE	RMSE	CRPS	INT	CVG	Time	Cores	Score
FRK	1.96	2.44	1.44	14.08	0.79	2.32	1	
Gapfill	1.33	1.86	1.17	34.78	0.36	1.39	40	
Lattice Krig	1.22	1.68	0.87	7.55	0.96	27.92	1	
Metakriging	2.08	2.50	1.44	10.77	0.89	2888.52	30	
MRA	1.33	1.85	0.94	8.00	0.92	15.61	1	
NNGP Conjugate	1.21	1.64	0.85	7.57	0.95	2.06	10	
NNGP Response	1.24	1.68	0.87	7.50	0.94	42.85	10	
Partition	1.41	1.80	1.02	10.49	0.86	79.98	55	
Pred. Proc.	2.05	2.52	1.85	26.24	0.75	640.48	1	
SPDE	1.10	1.53	0.83	8.85	0.97	120.33	2	
Tapering	1.87	2.45	1.32	10.31	0.93	133.26	1	
Periodic Embedding	1.29	1.79	0.91	7.44	0.93	9.81	1	
LAGP	1.65	2.08	1.17	10.81	0.83	2.27	40	-2.55
PALM	1.59	1.93	1.15	11.78	0.78	4.64	1	-2.85
Global + PALM	1.44	1.76	1.03	9.28	0.84	4.64	1	-2.39

Table 2: The original table from Heaton’s bake-off paper with added rows for PALM comparison, and an added column for the proper scoring rule

of “local” experts with data that is far removed from the central prediction location.

5.2 Michalewicz Function

For a final illustration consider the Michalewicz function (Molga and Smutnicki, 2005) in 3d. This is a good test function for PALM because it is highly non-stationary with large flat areas abutting drastic drops. As the number of dimensions increases, the number and severity of the dips also increases. For any number of dimensions, d , and steepness parameter m , the Michalewicz function is defined over $[0, \pi]^d$ as

$$f(\mathbf{x}) = - \sum_{i=1}^d \sin(x_i) \sin^{2m} \left(\frac{ix_i^2}{\pi} \right).$$

Because it is defined additively over inputs, a slice along any dimension will have the same shape regardless of its position in the other $d - 1$ dimensions. This allows one to intuit high dimensional dynamics visually by overlaying one-dimensional slices. Figure 15 shows slices created by the first three inputs. Any output in the 3d surface can be found by adding the x value for the individual dimensions with the corresponding point along that dimension’s line. The second panel shows a heat plot rendering in two dimensions, combining the first two slices from the left panel. The shape of the function in either direction remains the same regardless of the slice, although the depth of the slice changes.

To test the effectiveness of space-filling versus sequential designs for local experts in three dimensions, we generated a grid of forty points in 3d from the Michalewicz function, giving

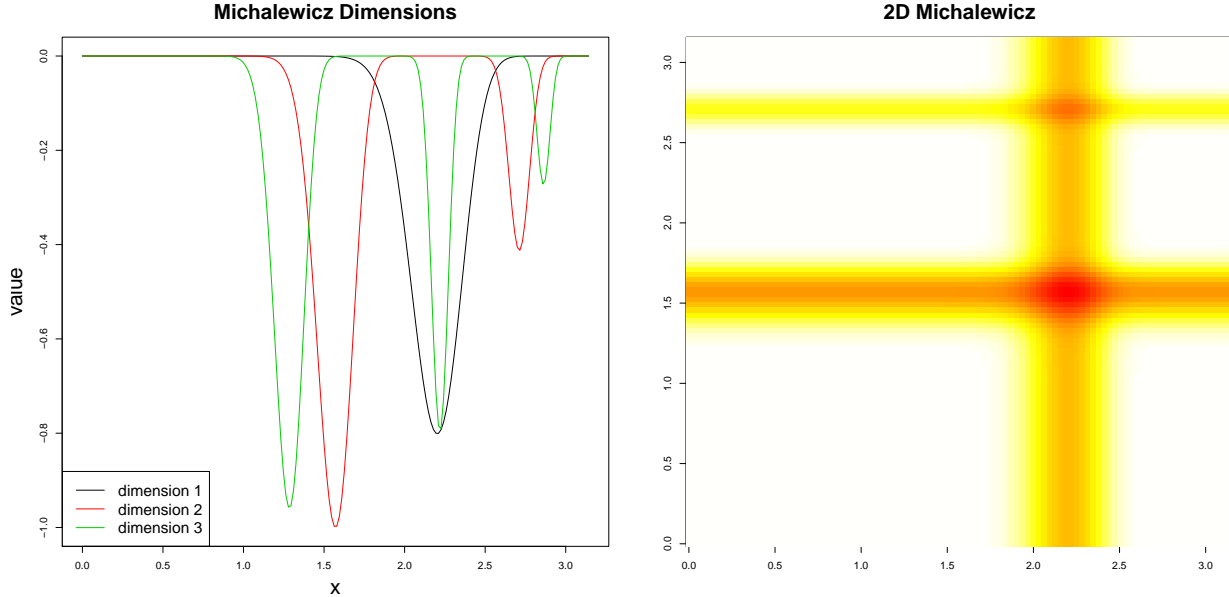


Figure 15: Left: The relative values of the first three dimensions of the Michalewicz function. The combined 3d surface can be reconstructed by adding points from these lines together. Right: a visualization of the Michalewicz function in 2d.

a total training data size of $N = 64,000$. We added $\mathcal{N}(0, \sigma^2 = 0.0025)$ noise to compare our methods in a stochastic setting. Finally the computational resources of both center selection methods were restricted to budgets of $K \in \{100, 200\}$, separately. The testing data set, over which PALMs were compared on RMSE and score, was generated the same way on a grid of size 39^3 . The entire process, from noise generation to center location selection, to fitting and prediction, was repeated one hundred times to get an accurate estimate of the comparison through Monte Carlo averaging.

	100 Centers		200 Centers	
	RMSE	Score	RMSE	Score
Spacefill	0.1237	3.5623	0.0878	4.1012
Sequential	0.1073	3.5704	0.0776	4.1212

Table 3: Average RMSE and Score for spacefilling models on 3d Michalewicz.

Focusing first on the $K = 100$ case, Table 3 shows that despite a notable improvement on RMSE for sequential over space-filling center selection, score is only slightly better. This is because the space-filled variation yields lower average variance. Note that the improvement in RMSE is still enough that the model scores better despite having higher variance, indicating that we have spent our computational resources wisely. When we increase the number of local experts to $K = 200$, the gap in RMSE closes slightly, while the difference in score becomes negligible. This confirms our instinct that sequential selection should be used in

situations where computational resources are limited.

6 Discussion

We have introduced a framework for local model averaging of Gaussian process predictors as an exemplar in a potentially wide class of such methods which we have dubbed PALM, for precision aggregated local models. The ingredients are a flexible local fit providing predictive means and variances, which we take from LAGP, and an aggregation scheme, which we take as inverse precision with adjustments for between-model covariance and overall ensemble size. We get all that while remaining in the class of GP regression – the resulting PALM-LAGP is a GP! Code to reproduce all of the results and plots used in this paper is open source and can be found in Gramacy Lab LAGP git repository.

<https://bitbucket.org/gramacylab/lagp/src/master/R/boosting>

It is easy to imagine other PALM instances. A number of other (locally applied) GP methods could be accommodated directly. We could swap the inverse squared exponential covariance function for other popular choices such as the Matern covariance, tapered or compactly supported covariance functions (Kaufman et al., 2008, 2011), or a non-stationary options (e.g., Ma et al., 2019). It would not significantly change the method to swap out a traditional Gaussian process for inducing points methods (Snelson and Ghahramani, 2006). Modern sparse spatial processes, such as a nearest neighbor GP (NNGP, Datta et al., 2016, 2015) can be swapped in. The only significant change to the PALM framework laid out above would be the necessity for a new sequential selection scheme without the existence of a “center” location for the local expert.

Even a simple linear model can be used as the local predictor. In the repository, the file `lmPALM.R` contains code that runs a PALM predictor using a third order linear approximation locally. The local experts are made by overlapping partitions of the input space for one and two dimensional examples: a sum of five randomly generated sine waves and Herbie’s tooth, respectively. Covariance is determined via empirical predictive correlation between the points used to build two models. These examples are made heteroskedastic by choosing a random point in the input space to be the center for radially increasing variance. Performance on both the mean and variance surfaces can be observed in the plots contained within. Additionally, the boundaries between any existing partition model, such as (Gramacy and Lee, 2008; Park and Apley, 2017), can be made smooth by applying the PALM weighting scheme.

Other embellishments to the wider framework naturally suggest themselves. For example, There is no reason why the greedy decisions of Section 4 could not be revisited later if computational resources permit. That is, we could entertain re-positioning those centers, either one at a time or on-mass, using the same score criterion. One way to implement that idea is to select a local expert for repositioning, which could be implemented by removing it from the ensemble and then following the same greedy sequential procedure for selecting a location to add it back in. We have experimented extensively with this “cycling” procedure, with code provided in the git repository. The idea was ultimately abandoned for presentation

in the main body of this manuscript because the removal process necessitates forming model predictions without each of the local expert models. This is an $O(K^3)$ procedure as the $O(K^2)$ predictive process must be repeated without each of the K centers.

We envision a number potential opportunities for statistical and computational performance gains. Exploiting independence in inferences in order to parallelize the computational flow is one such aspect, alluded to at length earlier. On statistical efficiency fronts, it may be beneficial to re-select the local designs for PALM’s local experts after the hyperparameters have been learned, e.g., using maximum likelihood estimates from LAGP. It may help to select a space filling design on the LAGP centers that is weighted in the input space based on the lengthscale parameters as well (Sun et al., 2019). Additionally, for some cases we may want to include variance explicitly in our sequential selection algorithm rather than exclusively picking center locations based on high residuals, and the idea that a relatively space filling point should have some marginal variance reducing properties.

Finally, there are a number of PALM tuning parameters that we set by intuition, but which could potentially be optimized. First, we selected $n = 50$ as the number of points a local model should be trained on, primarily because this is the default in the `laGP` package. Within the provided code, this can be changed by altering the defaults to the `aGP` function. Of course, users should be aware of the inverse quadratic relationship between predictive time and accuracy based on the size of local GP models. While the default we are using works well, it may be that other local model sizes may result in a better global model. One could imagine choosing such a tuning parameter via cross validation (CV). It may also possible to incorporate varying local model sizes in different areas of the input space that are easier or more difficult to capture. Updating local model size may be an alternative to sequential selection that allows the model to learn the relative complexity of the input space. Selection of the power to which weights are raised is another such tuning parameter. We chose to use $\log_d K$ as a slowly increasing function of the number of centers modulated for dimension of the input space. CV may well be a more data-centric option for that parameter as well. The LAGP repository provides code that that optimizes the predictive power for a specific model, but it runs slowly and offers little benefit to statistical efficiency.

References

- Binois, M., Gramacy, R. B., and Ludkovski, M. (2018). “Practical heteroscedastic gaussian process modeling for large simulation experiments.” *Journal of Computational and Graphical Statistics*, 27, 4, 808–821.
- Chen, T. and Ren, J. (2009). “Bagging for Gaussian process regression.” *Neurocomputing*, 72, 7, 1605–1610.
- Chipman, H., George, E., and McCulloch, R. (2010). “BART: Bayesian additive regression trees.” *The Annals of Applied Statistics*, 4, 1, 266–298.
- Chipman, H., Ranjan, P., and Wang, W. (2012). “Sequential design for computer exper-

- iments with a flexible Bayesian additive model.” *Canadian Journal of Statistics*, 40, 4, 663–678.
- Cochran, W. G. (1954). “The Combination of Estimates from Different Experiments.” *Biometrics*, 10, 1, 101–129.
- Cohn, D. (1994). “Neural network exploration using optimal experiment design.” In *Advances in neural information processing systems*, 679–686.
- Cressie, N. (1991). *Statistics for Spatial Data*, revised edition. John Wiley and Sons, Inc.
- Cressie, N. and Johannesson, G. (2008). “Fixed Rank Kriging for Very Large Data Sets.” *Journal of the Royal Statistical Society, Series B*, 70, 1, 209–226.
- Datta, A., Banerjee, S., Finley, A. O., and Gelfand, A. E. (2016). “Hierarchical Nearest-Neighbor Gaussian Process Models for Large Geostatistical Datasets.” *Journal of the American Statistical Association*, 111, 514, 800–812.
- Datta, A., Banerjee, S., Finley, A. O., Hamm, N. A. S., and Schaap, M. (2015). “Non-separable Dynamic Nearest-Neighbor Gaussian Process Models for Large spatio-temporal Data With an Application to Particulate Matter Analysis.” *arXiv:1510.07130 [stat]*. ArXiv: 1510.07130.
- Furrer, R., Genton, M., and Nychka, D. (2006). “Covariance Tapering for Interpolation of Large Spatial Datasets.” *Journal of Computational and Graphical Statistics*, 15, 502–523.
- Gneiting, T. and Raftery, A. (2007). “Strictly Proper Scoring Rules, Prediction, and Estimation.” *Journal of the American Statistical Association*, 102, 477, 359–378.
- Goldberg, P. W., Williams, C. K., and Bishop, C. M. (1998). “Regression with input-dependent noise: A Gaussian process treatment.” In *Advances in Neural Information Processing Systems*, vol. 10, 493–499. Cambridge, MA: MIT press.
- Gramacy, R. and Apley, D. (2015). “Local Gaussian process approximation for large computer experiments.” *Journal of Computational and Graphical Statistics*, 24, 2, 561–578.
- Gramacy, R. and Lee, H. (2008). “Bayesian treed Gaussian process models with an application to computer modeling.” *Journal of the American Statistical Association*, 103, 483, 1119–1130.
- Gramacy, R., Niemi, J., and Weiss, R. (2014). “Massively parallel approximate Gaussian process regression.” *SIAM/ASA Journal on Uncertainty Quantification*, 2, 1, 564–584.
- Gramacy, R. and Polson, N. (2011). “Particle Learning of Gaussian Process Models for Sequential Design and Optimization.” *Journal of Computational and Graphical Statistics*, 20, 1, 102–118.

- Gramacy, R. B. (2016). “laGP: Large-Scale Spatial Modeling via Local Approximate Gaussian Processes in R.” *Journal of Statistical Software*, 72, 1.
- (2020). *Surrogates: Gaussian Process Modeling, Design and Optimization for the Applied Sciences*. Boca Raton, Florida: Chapman Hall/CRC. <http://bobby.gramacy.com/surrogates/>.
- Haaland, B. and Qian, P. (2011). “Accurate Emulators for Large-Scale Computer Experiments.” *Annals of Statistics*, 39, 6, 2974–3002.
- Heaton, M. J., Datta, A., Finley, A. O., Furrer, R., Guinness, J., Guhaniyogi, R., Gerber, F., Gramacy, R. B., Hammerling, D., Katzfuss, M., et al. (2019). “A case study competition among methods for analyzing large spatial data.” *Journal of Agricultural, Biological and Environmental Statistics*, 24, 3, 398–425.
- Johnson, M., Moore, L., and Ylvisaker, D. (1990). “Minimax and maximin distance designs.” *Journal of statistical planning and inference*, 26, 2, 131–148.
- Katzfuss, M. (2017). “A multi-resolution approximation for massive spatial datasets.” *Journal of the American Statistical Association*, 112, 517, 201–214.
- Katzfuss, M. and Guinness, J. (2018). “A general framework for Vecchia approximations of Gaussian processes.” *arXiv preprint arXiv:1708.06302*.
- Kaufman, C., Bingham, D., Habib, S., Heitmann, K., and Frieman, J. (2012). “Efficient Emulators of Computer Experiments using Compactly Supported Correlation Functions, with An Application to Cosmology.” *The Annals of Applied Statistics*, 5, 4, 2470–2492.
- Kaufman, C. G., Bingham, D., Habib, S., Heitmann, K., and Frieman, J. A. (2011). “Efficient emulators of computer experiments using compactly supported correlation functions, with an application to cosmology.” *The Annals of Applied Statistics*, 5, 4, 2470–2492. ArXiv: 1107.0749.
- Kaufman, C. G., Schervish, M. J., and Nychka, D. W. (2008). “Covariance Tapering for Likelihood-Based Estimation in Large Spatial Data Sets.” *Journal of the American Statistical Association*, 103, 484, 1545–1555.
- Kim, H., Mallick, B., and Holmes, C. (2005). “Analyzing nonstationary spatial data using piecewise Gaussian processes.” *Journal of the American Statistical Association*, 100, 470, 653–668.
- Lee, H., Gramacy, R., Linkletter, C., and Gray, G. (2011). “Optimization subject to hidden constraints via statistical emulation.” *Pacific Journal of Optimization*, 7, 3, 467–478.
- Lloyd, S. P. (1982). “Least squares quantization in PCM.” *IEEE Transactions on Information Theory*, 28, 2, 129–137.

- Ma, P., Kang, E. L., Braverman, A., and Nguyen, H. (2019). “Spatial Statistical Downscaling for Constructing High-Resolution Nature Runs in Global Observing System Simulation Experiments.” *Technometrics*, 61, 3, 322–340.
- Molga, M. and Smutnicki, C. (2005). “Test Functions for Optimization Needs.”
- Neal, R. (1998). “Regression and classification using Gaussian process priors.” *Bayesian Statistics*, 6, 475.
- Nychka, D., Wikle, C., and Royle, J. (2002). “Multiresolution Models for Nonstationary Spatial Covariance Functions.” *Statistical Modelling*, 2, 315–331.
- Park, C. and Apley, D. (2017). “Patchwork Kriging for Large-scale Gaussian Process Regression.” *arXiv:1701.06655 [cs, stat]*. ArXiv: 1701.06655.
- Park, C. and Huang, J. Z. (2016). “Efficient Computation of Gaussian Process Regression for Large Spatial Data Sets by Patching Local Gaussian Processes.” *Journal of Machine Learning Research*, 17, 174, 1–29.
- Park, C., Huang, J. Z., and Ding, Y. (2011). “Domain Decomposition Approach for Fast Gaussian Process Regression of Large Spatial Data Sets.” *Journal of Machine Learning Research*, 12, May, 1697–1728.
- Quiñonero–Candela, J. and Rasmussen, C. (2005). “A Unifying View of Sparse Approximate Gaussian Process Regression.” *Journal of Machine Learning Research*, 6, 1939–1959.
- Rasmussen, C. E. and Williams, C. K. I. (2006). *Gaussian Processes for Machine Learning*. The MIT Press.
- Rushdi, A., P. Swiler, L., T. Phipps, E., D’Elia, M., and Ebeida, M. (2016). “VPS: Voronoi Piecewise Surrogate Models for High-Dimensional Data Fitting.” *International Journal for Uncertainty Quantification*, 7.
- Sacks, J., Welch, W. J., Mitchell, T. J., and Wynn, H. P. (1989). “Design and Analysis of Computer Experiments.” *Statistical Science*, 4, 409–435.
- Sang, H. and Huang, J. Z. (2012). “A Full Scale Approximation of Covariance Functions for Large Spatial Data Sets.” *Journal of the Royal Statistical Society: Series B*, 74, 1, 111–132.
- Santner, T., Williams, B., and Notz, W. (2018). *The Design and Analysis of Computer Experiments, Second Edition*. New York, NY: Springer–Verlag.
- Snelson, E. and Ghahramani, Z. (2006). “Sparse Gaussian Processes using Pseudo-inputs.” In *Advances in Neural Information Processing Systems*, 1257–1264. MIT press.

- Sun, F., Gramacy, R. B., Haaland, B., Lawrence, E., and Walker, A. (2019). “Emulating satellite drag from large simulation experiments.” *SIAM/ASA Journal on Uncertainty Quantification*, 7, 2, 720–759.
- Tresp, V. (2000). “A Bayesian Committee Machine.” *Neural Computation*, 12, 11, 2719–2741.
- Vapnik, V. (2013). *The nature of statistical learning theory*. Springer science & business media.